Fabrication of a versatile aptasensing chip for aflatoxin B1 in photothermal and electrochemical dual modes

Chengquan Wang (wangcq@ujs.edu.cn)
Jiangsu University
Xin Zhao
Jiangsu University
Chengdong Gu
Jiangsu University
Foyan Xu
Jiangsu University
Wuhao Zhang
Jiangsu University
Xingyi Huang
Jiangsu University
Jing Qian
Jiangsu University

Research Article

Keywords: Food Safety, Aptasensor, Aflatoxin B1, Photothermal analysis, Dual modes

Posted Date: April 20th, 2022

DOI: https://doi.org/10.21203/rs.3.rs-1556230/v1

Abstract

The dual-mode sensing strategy not only has the inherent characteristics of each response mode, but also can mutually verify the detection results obtained by different modes, which will effectively improve the accuracy and reliability of detection. The electrochemical-photothermal dual-mode not only has two mode signals, but also has the advantages of fast response, high sensitivity, good selectivity, low cost and simple operation. Efficient integration and accurate detection of pathogenic bacteria to achieve early warning of food safety is one of the most valuable antifouling methods. Here, we report an integrated design strategy to establish a photothermal and electrochemical dual modes for sensitive detection of aflatoxin B1 (AFB1). The aptasensor was fabricated by loading the Au@Fe_3O_4 onto the indium tin oxides (ITO) conductive glass modified AuNPs nano-layer (ITO/AuNPs) surface through DNA hybridization between aptamer and cDNA. After adding AFB1, aptamer tends to form aptamer-AFB1 complex, resulting in part of Au@Fe_3O_4 falling off the ITO/AuNPs surface and entering the reaction solution. 3,3',5,5'-tetramethylbenzidine (TMB) and H_2O_2 system produces color change under the catalysis of Au@Fe_3O_4 and realizes the conversion of light and heat under the excitation of near-infrared light. Photothermal signal analysis is realized with the help of thermometer. In addition, combined with electrochemical impedance spectroscopy analysis with ITO/AuNPs electrode, a dual channel method is provided for AFB1 detection. Under the optimal conditions, the developed aptasensor realized sensitive and specific detection of AFB1 from 10 pg mL^{-1} to 300 ng mL^{-1} with low detection limit of 5 pg mL^{-1} in photothermal mode. Importantly, this work provided a promising prospect for the application of photothermal effect coupled with electrochemical aptasensor in food safety.

1. Introduction

Aflatoxin B1 (AFB1) is the most toxic in naturally contaminated foods (Wang et al., 2018), which can cause liver cancer and even death to human beings and animals (Bashiry et al., 2021; Ahmad Al-Jaal et al., 2019; Buszewska-Forajta et al., 2020). Considering its carcinogenic effects on human beings, many countries have established the maximum level of AFB1 between 0.05 and 20 ng mL^{-1} in all food and agriculture products (Babu et al., 2011). The European Union stipulates that the content of aflatoxin B1 in human consumer goods shall not exceed 2 μg kg^{-1} (Goud et al., 2016). The research on food safety related to aflatoxin B1 has attracted the favor of the majority of researchers and made a series of research progress, such as chromatography and immunoassay (Xing et al., 2020; Xia et al., 2018; Xiong et al., 2018). The methods mentioned above can accurately and sensitively detecttion aflatoxin B1, but the defects of time-consuming and high detection cost limit their development (Xue et al., 2019; Xiong et al., 2020). Therefore, it is urgent to develop an efficient AFB1 detection method (Wang et al., 2019).

Since the advent of aptamers in the 1990s, researchers have worked hard to the research of aptamers with many advantages (Liu et al., 2018; Chen et al., 2017a). The special spatial configuration of aptamers is easy to form different three-dimensional structures, such as spiral, hairpin, stem ring, convex ring and other structures, which can easily capture the target based on the interaction of various functional groups

(Yang et al., 2018; Barthelmebs et al., 2011; Zhang et al., 2012). Compared with antibody detection, the aptamer obtained by screening are easier to prepare and store (Hansen et al., 2006; Wang et al., 2016a). Nowadays, Various aptasensor methods came into being and were successfully applied to the efficient detection of aflatoxin B1, such as colorimetric, electrochemistry, and fluorescent aptasensors (Hao et al., 2018; Seok et al., 2015; Luo et al., 2019; Zheng et al., 2016). Among them, the colorimetric system (3,3',5,5'-tetramethylbenzidine (TMB) and H_2O_2) mediated by F_3O_4 is considered to be one of the most promising technologies for the determination of AFB1 because it can usually change the color in the process of colorimetric analysis (Woo et al., 2013; Fu et al., 2018). Some reports have proved that TMB-H_2O_2 colorimetric system has high light-heat conversion efficiency when activated by near infrared (NIR), which means that TMB-H_2O_2 system has the potential of AFB1 detection by photothermal analysis (Luo et al., 2020b). The previous research results of our research group have proved that the enzyme like catalytic activity of Au@Fe_3O_4 is 1.5 times that of Fe_3O_4, which greatly increases the sensitivity of the sensor (Wang et al., 2016b). However, the above single detection mode will inevitably be affected by the possible simultaneous interferences, different operators, instruments and non-standard detection processes. The dual-mode sensing strategy not only has the inherent characteristics of each response mode, but also can mutually verify the detection results obtained by different modes, which will effectively improve the accuracy and reliability of detection (Fu et al., 2021).

The electrochemical-photothermal dual-mode not only has two mode signals, but also has the advantages of fast response, high sensitivity, low cost and simple operation. Here, a versatile aptasening chip researched for the photothermal and electrochemical dual modes sensitive detection of AFB1 in this work. Compared with single-mode electrochemical signal, photothermal signal can effectively improve the accuracy and reliability of detection, and achieve mutual verification and joint use. ITO conductive glass modified AuNPs nano-layer (ITO/AuNPs) can not only effectively improve the electronic conductivity, but also effectively link the thiol terminal modified aptamer. The aptasensor fabricated by loading the Au@Fe_3O_4 onto the ITO/AuNPs surface obtained by hybridization of aptamer and cDNA. After adding AFB1, aptamer tends to form aptamer-AFB1 complex, resulting in part of Au@Fe_3O_4 falling off the ITO/AuNPs surface and entering the reaction solution. TMB-H_2O_2 system with magnetically collected Au@Fe_3O_4 produces color change under the catalysis of Au@Fe_3O_4 and photothermal signal analysis under the excitation of near infrared light realized with the help of thermometer. In addition, combined with electrochemical impedance spectroscopy (EIS) analysis with ITO/AuNPs electrode, a dual mode provided for AFB1 detection.

2. Experimental Section

2.1. Reagents and Apparatus

Diethylene glycol (DEG), glutaraldehyde, ethylene glycol (EG), $HAuCl_4 \cdot 4H_2O$, $FeCl_3 \cdot 6H_2O$, (3-aminopropyl) triethoxysilane (APTS), and polyethylene glycol (PEG) got from Sinopharm Chemical Reagent Co., Ltd. (Beijing, China). OTA, Tris (2-chloroethyl) phosphate (TCEP), aflatoxins B1 (AFB1), 3,3',5,5'-

tetramethylbenzidine (TMB), fumonisin B1 (FB1), and 6-mercapto-1-hexanol (MCH) got from Sigma-Aldrich. 5'-GAT CGG GTG TGG GTG GCG TAA AGG GAG CAT CGG ACA-SH-3'(aptamer) (Chrysels, et al. 2011; Chen, et al. 2017b) and 5'-CCT TTA CGC CAC CCA CAC CCG ATC-NH_2-3' (cDNA) were purchased from Sangon Biotech Co., Ltd. (Shanghai, China).

The morphologies of samples were observed with the help of transmission electron microscopy (TEM) (HitachS-2400N, Japan). A three-electrode system is composed of ITO conductive glass modified gold working electrode, Ag/AgCl as reference electrode and platinum wire as counter electrode. X-ray photoelectron spectroscopy (XPS) obtained by ESCALAB 250 multi technology surface analysis system of Waltham thermal power company in Massachusetts. UV – vis spectra were obtained on a UV-2450 spectrophotometer (Shimadzu, Tokyo, Japan). A diode laser with output power from 0 to 2.5 W and wavelength of 808 nm was purchased from Yuanming Laser Technology Co., Ltd (Ningbo). An ordinary digital thermometer was purchased from Boyang Instrument Co., Ltd (Zhengzhou).

2.2. Synthesis of Au@Fe_3O_4 nano-heterojunction

The Au@Fe_3O_4 nano-heterojunction was prepared by one-step hydrothermal method, which was previously reported by our group (Wang et al., 2016b). Typically, 2 mmol of $FeCl_3 \cdot 6H_2O$ was ultrasonically dispersed in 20 mL of mixture containing EG and DEG (volume ratio of 1:1). Subsequently, sodium acetate and PEG (1.5 g and 1 g) were poured into the above mixture with stirring for 30 min. Finally, $HAuCl_4$ (2%, 0.5 mL) was injected into the above solution, stirring for 30 min and transferred to a hydrothermal reactor for reaction at 200°C for 6 hours. The obtained Au@Fe_3O_4 nano-heterojunction (MB) were washed in water and alcohol with the help of magnets for many times, which was dispersed in 40 mL of ethanol in refrigerator for future use.

2.3. Preparation of complementary DNA conjugated Au@Fe_3O_4 nano-heterojunction

The complementary DNA (cDNA) conjugated MB (cDNA-MB) mainly referred to our previous preparation method (Wang et al., 2015a). In short, 0.5 mL of APTS was added with 20 mL of MB prepared above, and after continuous stirring for 1 hour, the amino-terminated MB was successfully prepared after repeated water and alcohol washing. Next, 5 mL of glutaraldehyde added to 20 mL of the above product, shaken at 37°C for 2 hours and purified several times. Finally, 100 μL cDNA was added to the above solution with shaking for 2 hours. After purification, cDNA-MB was successfully prepared and re-dispersion in 20 mL of Tris HCl buffer (10 mM) for future use.

2.4. Preparation of ITO conductive glass substrate with Au plating layer

The pre-treatment of ITO electrode was performed by the following procedure. Firstly, the ITO electrodes (1.5×2 cm^2) were sonicated orderly in dilute ammonia water, ethanol, and water for 10 min, respectively. Then, the ITO electrodes were dried under infrared light, and the perforated brown tape with a square hole

(The sides of the square are 1 cm) was covered on the surface of ITO electrodes. The electrodeposition of Au NPs on ITO was carried out in 2 mM $HAuCl_4$ using the cyclic voltammetry (CV) for 30 cycles (potential range: -0.2 to 1.2 V, scan rate of 100 mV s^{-1}). After washing with water and dried under nitrogen stream, the Au NPs modified ITO (ITO/AuNPs) was then obtained.

2.5. Preparation of aptamer conjugated of ITO conductive glass substrate with AuNPs

250 μL aptamer (Apt,100 μM) solution was fully mixed with Tris-HCl buffer (10 mM) containing TCEP (100 mM), and purified after shaking at 37°C for 1 h to remove excess TCEP. Thirdly, ITO conductive glass substrate with AuNPs plating layer (ITO/AuNPs) were purified by ultrasound for 30 seconds, incubated with the activated aptamer for 30 minutes. Finally, after purification, salt aging and MCH, the prepared Apt-ITO/AuNPs is immersed into Tris-HCl buffer (10 mM), stored in refrigerator for future use (Wang et al., 2015b).

2.6. Preparation of the aptasensor

After shaking the mixture of cDNA-MB and Apt-ITO/AuNPs for 1 hour at 37°C, the multifunctional aptasensor MB-cDNA/Apt-ITO/AuNPs was successfully prepared after purification, which was immersed in Tris-HCl buffer (10 mM) and stored a in refrigerator for standby.

2.7. Assay procedure

The aptasensor of MB-cDNA/Apt-ITO/AuNPs was initially rinsed with ABS buffer, dried with nitrogen. The aptasensor was immersed in 3 mL different concentrations of AFB1 standard solution for 30 min at 4°C. Then, the aptasensor was used as a working electrode for the EIS measurement in 2 mL electrolyte solution including the redox probe $[Fe(CN)_6]^{3-/4-}$. With the help of a magnet, the cDNA-MB collected from the reaction solution is transferred to a centrifuge tube containing TMB-H_2O_2 solution. Finally, the temperature of the blue solution after reaction was measured by thermometer after illumination at 808 nm for 20 s.

3. Results And Discussion

3.1. Characterization of the Au@Fe_3O_4 nano-heterojunction

This kind of $Au_{(core)}@Fe_3O_{4(shell)}$ nano-heterojunction not only has strong magnetism, but also has stronger catalytic performance than pure Fe_3O_4 nanoparticles, which can be proved from our previous reports (Wang et al., 2016b). It can be seen from Fig. 1A and 1B that the dark AuNPs ball occupies the center of the whole ball, with a diameter of 30 nm, surrounded by slightly lighter Fe_3O_4, with a diameter of 130 nm. The XRD (Fig. 1C) further proved the successful preparation of the Au@Fe_3O_4 nano-heterojunction. The Au@Fe_3O_4 has four more diffraction peaks, which are 38.1°, 44.3°, 64.5°, and 77.6° ascribed to the (111), (200), (220), and (311) planes (curve a) for the AuNPs of face-centered-cubic

(JCPDS No. 04-0784) (curve c) compared with the XRD diffraction peaks of pure Fe_3O_4 (curve b). The Au@Fe_3O_4 nanoparticles we prepared have the same typical ferromagnetism as pure Fe_3O_4, with small magnetic permanence and coercively. As can be seen from Fig. 1D, the saturation magnetism of ferromagnetic material is 50.2 emu g^{-1} (curve b), less than that of pure Fe_3O_4 (35 emu g^{-1}) (curve a), which is mainly due to the integration of AuNPs. It can also find that the Au@Fe_3O_4 could quickly concentrate around the magnet and could be quickly and uniformly dispersed by hand shaking in 3 seconds (inset of Fig. 1D), showing that the Au@Fe_3O_4 has very similar properties to superparamagnetic particles (Xie et al., 2010).

Here Fig. 1

3.2. Characterization of the complementary DNA conjugated Au@Fe_3O_4 nano-heterojunction

cDNA can be successfully connected to the surface of Au@Fe_3O_4 mainly through condensation reaction. According to our previous research results (Wang et al., 2016b), the Au@Fe_3O_4 surface has a large number of hydroxyl groups, and the cDNA end is modified with amino groups. With the help of glutaraldehyde, the cDNA is successfully connected to the Au@Fe_3O_4 surface. We can support this conclusion by UV absorption spectrum. Figure 2A shows that curve a, b are the UV absorption spectra of cDNA and Au@Fe_3O_4 respectively. Observing curve c, there are corresponding characteristic peaks of cDNA and Au@Fe_3O_4 at 265 and 585 nm, indicating that cDNA is successfully connected to the surface of Au@Fe_3O_4.

Here Fig. 2

3.3. Fabrication the aptamer conjugated ITO conductive glass substrate with AuNPs

The CV_S in 0.5 M H_2SO_4 solution proved that the ITO conductive glass layer was successfully plated with AuNPs layer, in which the scanning potential range was 0 to 2 V. Compared with the CV of bare ITO electrode (curve a of Fig. 2B), there are oxidation peak and reduction peak of AuNPs at 1.2V and 0.6V, respectively. (curve b of Fig. 2B) (Wang et al., 2018). Aided by Au-S linkage, the aptamer is connected to the AuNPs modified electrode surface, which can be seen from the Fig. 2C. The XPS spectrum of the electrode modified with aptamer has an obvious P 2p characteristic peak (curve b), which is mainly due to the existence of phosphate skeleton in aptamer, and the center of the peak is at 133.3 eV. In contrast, the XPS spectrum of the electrode without modified aptamer had no characteristic peak of P 2p (curve a).

3.4. Preparation of the multifunctional aptasensor

The above data show that we successfully modified the aptamer to the electrode surface. However, the maximum load of aptamer per unit area and the time required are two important parameters. Figure 2D shows the electrode impedance value of modified aptamer increases with the increase of aptamer

concentration. When the concentration of aptamer reaches 1 μM, the impedance value reaches the highest platform. Therefore, we selected the aptamer as 1 μM for the best loading concentration.

Figure 3A shows the relationship between loading time and impedance value when the fixed concentration of aptamer is 1 μM. It can be seen that the impedance value increases with the extension of loading time, but the impedance value increases slowly after 12 h. Therefore, we chose 12 h as the time for the aptamer loading on ITO/AuNPs in this study.

Under the optimization condition, the multifunctional aptasensor connects the cDNA-MB to the Apt-ITO/AuNPs based on the base matching principle between the aptamer and its complementary chain. The step-by-step preparation process of the electrode is completed by monitoring the impedance value of $[Fe(CN)_6]^{3-/4-}$ (Fig. 3B). The inset of Fig. 3B shows the classic Randles equivalent circuit. It can be seen from the Nyquist plots that any fabrication steps of the electrode will be reflected by the change of the semicircle diameter of R_{et}. Because the electron transfer process of the redox probe on the modified electrode surface is blocked, the interface R_{et} increases sharply from 350 Ω (curve a) to 950 Ω (curve b) after the aptamer linked on the ITO/AuNPs. After MCH treatment, the Ret value was changing to be 1750 Ω (curve c) (Wang et al., 2015a). Finally, when cDNA-MB was modified to the Apt-ITO/AuNPs, the R_{et} increased to 3600 Ω (curve d). In order to clarify the maximum concentration of loaded cDNA-MB per unit area of ITO/AuNPs, we use the EIS value of $[Fe(CN)_6]^{3-/4-}$ to monitor the change trend of loaded concentration of cDNA-MB (Fig. 3C). With the continuous increase of cDNA-MB concentration (from 0.1 to 5 μL mL^{-1}), the impedance diameter also increases. Finally, when the MB concentration is 5 μL mL^{-1}, the impedance diameter no longer increases. Therefore, we choose the concentration of MB as 5 μL mL^{-1} as the most optimal load. As can be seen from Fig. 3D, the optimum temperature and time for the reaction of the prepared electrode with 50 pg mL^{-1} AFB1 are 37°C and 60 minutes, respectively.

Here Fig. 3

3.5. Fabrication of the aptasensor and its working principle

ITO conductive glass is an important substrate for the successful construction of aptasensor. Its conductive layer modified AuNPs nano-layer can not only effectively improve the electronic conductivity, but also effectively link the thiol terminal modified aptamer. See Scheme 1 for the detailed preparation: Firstly, thiol terminal modified aptamers were modified on ITO/AuNPs surface by Au-S bond. Then, MCH was introduced to block redundant reaction sites of ITO/AuNPs. Our previous studies showed that the surface of MB was rich in hydroxyl groups (Wang et al., 2016b), and the terminal of cDNA was modified with amino groups. With the help of glutaraldehyde, cDNA was successfully connected to the surface of MB. Finally, ITO/AuNPs-Apt/cDNA-MB aptasensor was successfully obtained at 37°C with the help of the specific reaction between aptamer and cDNA. When the aptasensor prepared here is immersed in the solution to be tested containing the target AFB1, AFB1 and its aptamer specifically preferentially bind to promote the separation of cDNA-MB from ITO/AuNPs into the solution to be tested. With the increase concentration of AFB1, the amount of cDNA-MB in the solution to be tested increases. At this time, use a

magnet to collect cDNA-MB in the solution to be measured, and then add it to the ABS solution containing TMB and H_2O_2. Previous studies have shown that MB has peroxidase like enzyme, so cDNA-MB can catalyze H_2O_2 and oxidize TMB to make it blue. The greater the concentration of cDNA-MB, the darker the blue. The temperature of blue solution does not change under the irradiation of 808 nm laser. At this time, the temperature change is recorded by thermometer. The aptasensor was then used to make a three-electrode system into electrolyte solution including the redox probe for EIS measurements.

Here Scheme 1

3.6. Optimization of parameters

To clarify the catalytic performance of MB for TMB and H_2O_2, we use Vis-NIR spectroscopy to help us analyze the results. As displayed in Fig. 4A, in the absence of cDNA-MB, the visible near infrared absorption of TMBox can be observed at 650 and 890 nm, indicating that MB nanoenzyme has oxidase like activity. With the increase of MB concentration from 5 μM to 50 μM, the above characteristic absorbance increases to a maximum and stops. It is well known that a class of nano materials with enzyme catalytic activity cannot oxidize TMB to TMBox under neutral conditions, high temperature and short time. Figure 4B and 4C show that the optimum temperature, reaction time and pH value of MB catalytic system are 37°C, 15 minutes and 4, respectively. Furthermore, the blue solution after the reaction was placed under 808 nm laser beam to obtain the optimal irradiation time. Figure 4D shows that the temperature elevation range increases with the increase of irradiation time (range of 0 ~ 5 min), but turned down at 10 min. The temperature does not rise but decreases, which can be attributed to the photo-bleaching of TMBox during long-term irradiation (Zheng et al., 2013; Cheng et al., 2013). Thus, 5 min was used as the irradiation time in this study to avoid the photo bleaching for the aptasensor.

Here Fig. 4

3.7. Linear range of the aptasensor

Under the above conditions, the sensitivity of the aptasensor for AFB1 detection was investigated. As shown in Fig. 5A, with the increase of AFB1 concentration, the impedance radius of aptasensor decreases. The linear relationship between *R*et value and AFB1 concentration and the relationship between $\triangle R$et ($\triangle R$et = *R*et- $R\text{et}_0$) value and logarithm of AFB1 concentration are shown in Fig. 5B. The linear equation is as follows: $\triangle R\text{et} = -2734 - 1360 \lg (c/\text{ng ml}^{-1})$ ($R^2 = 0.996$), and the concentration range is 50 pg ml^{-1}-500 ng ml^{-1}. The limit of detection (LOD) is calculated as 25 pg ml^{-1}, which is much lower than the determined maximum tolerance level of AFB1 in food and feed based on S/N = 3. The aptasensor has a good linear relationship between temperature increases ($\triangle T = T\text{-}T_0$) with the logarithm of target AFB1 concentration range from 10 pg ml^{-1}-300 ng ml^{-1} ($R^2 = 0.994$) (Fig. 5C). The LOD was calculated to be 5 pg ml^{-1}, which was lower than the reported colorimetric sensor (Yang et al., 2011; Pradhan et al., 2007) (Fig. 5D). Table 1 lists the detection results of aflatoxin B1 by relevant aptasensors. It can be seen that the aptasensor we developed has a wider detection range than other sensors (Wang et al., 2018; Chen et al., 2017b; Xie et al., 2014).

Table 1
Comparison of the analytical performance of other aptasensors developed for AFB1 determination.

Methods	Liner range (ng mL^{-1})	LOD (ng mL^{-1})	References
Colorimetric	8–250	8	Yang, et al. 2011
	0.0004–20	0.00012	Xie, et al. 2014
EIS	0.03–3.3	0.13	Pradhan, et al. 2007
	0.02-50	0.015	Wang, et al. 2018
	0.03-33	0.02	Chen, et al. 2017b
Photothermal	0.001–300	0.0005	This work
Electrochemical impedance spectroscopy (EIS)			

Here Fig. 5

3.8. Selectivity and reproducibility

In order to verify that the aptasensor has specificity only for AFB1, the aptasensors reacted with the targets (AFB1, OTA, OTB, FB1 and AFM1). The cDNA-MB collected by the magnet is added to the reaction solutions with TMB and H_2O_2, only the reaction system added with AFB1 has obvious blue change, indicating that the aptasensor has specific selection for AFB1 (Inset of Fig. 4D). We performed five AFB1 repeated measurements with a relative standard deviation (RSD) of less than 5.1%.

Here Table 1

3.9. Application

We applied the aptasensor to the photothermal detection of AFB1 in peanut samples, and the detection results are shown in Table 2. We selected three different contaminated peanut samples with AFB1 concentrations of 0.1, 1 and 10 ng mL^{-1}, respectively. The recovery of AFB1 is 96% ~ 97%, and the RSD value of the recovery is less than 6.3%, which show that the photothermal aptasensor can be used for the determination of AFB1 in peanut samples.

Table 2
Results of AFB1 detection in peanut samples by photothermal aptasensor (n = 5).

Sample	Spiked (ng mL^{-1})	Detected (ng mL^{-1})	RSD (%)	Recovery (%)
1	0.1	0.096 ± 0.006	6.3	96.0
2	1	0.97 ± 0.05	5.2	97.0
3	10	9.6 ± 0.4	4.2	96.0

Here Table 2

4. Conclusions

In this work, a versatile aptasensing chip was proposed for the detection of AFB1 in photothermal and electrochemical dual modes. Using the advantages of multi-functional signal probe and near-infrared laser irradiation, the aptasensor realizes the non-contact and accurate control of the signal. In addition, combined with electrochemical impedance detection technology, this method realizes the dual channel synchronous detection of AFB1, which increases the accuracy and selectivity of detection. Photothermal induced technology is a promising method to realize high-sensitivity signal amplification. Therefore, the combination of photothermal technology and other detection methods to meet the needs of food safety is the development trend in the future.

Declarations

Data Availability

The datasets generated during and/or analyzed during the current study are available from the corresponding author on reasonable request.

Code Availability

Not applicable.

Funding

We thank for supporting by the Project of Faculty of Agricultural Equipment of Jiangsu University (No. NZXB20200211 and No. NZXB20210208), National Natural Science Foundation of China (No. 21976071), and Jiangsu University Fund (No. 19JDG025).

Author information

Affiliations

Jiangsu University, Zhenjiang 212013, China

Contributions

Chengquan Wang: Supervision, conceptualization, methodology, investigation, data curation, writing-review & editing. Xin Zhao: Investigation, data curation & writing-original draft. Chengdong Gu: Preparation electrode chip. Foyan Xu: Sample pretreatment. Wuhao Zhang: Writing-review & editing. Xingyi Huang: Supervision, conceptualization, investigation, data curation. Jing Qian: Supervision, conceptualization, methodology, investigation, data curation, writing-review & editing.

Corresponding author

Correspondence to Chengquan Wang, Xingyi Huang, or Jing Qian.

Ethics declarations

Informed Consent

Informed consent not applicable.

Conflict of Interest

The authors declare no competing interests.

Additional information

Publisher's Note

References

1. Ahmad Al-Jaal B, Jaganjac M, Barcaru A, Horvatovich P, Latif A (2019) Aflatoxin, fumonisin, ochratoxin, zearalenone and deoxynivalenol biomarkers in human biological fluids: A systematic literature review, 2001–2018. Food and Chemical Toxicology 129: 211–228.
2. Babu D, Muriana P (2011) Immunomagnetic bead-based recovery and real time quantitative PCR (RT iq-PCR) for sensitive quantification of aflatoxin B1. Journal of Microbiological Methods 86: 188–194.
3. Barthelmebs L, Jonca J, Hayat A, Beatriz P, Marty JL (2011) Enzyme-Linked Aptamer Assays (ELAAs), based on a competition format for a rapid and sensitive detection of ochratoxin A in wine. Food Control 22: 737–743.
4. Bashiry M, Javanmardi F, Sadeghi E, Shokri S, Hossieni H, Oliveira C, Khaneghah A (2021) The prevalence of aflatoxins in commercial baby food products: A global systematic review, meta-analysis, and risk assessment study. Trends in Food Science & Technology 114: 100–115.
5. Buszewska-Forajta M (2020) Mycotoxins, invisible danger of feedstuff with toxic effect on animals. Toxicon 182: 34–53.
6. Chen L, Wen F, Li M, Guo X, Li S, Zheng N, Wang J (2017) A simple aptamer-based fluorescent assay for the detection of Aflatoxin B1 in infant rice cereal. Food Chemistry 215: 377–382.
7. Chen XX, Che CP, Korolchuk VI, Gan F, Pan C, Huang K (2017) Selenomethionine alleviates AFB1-induced damage in primary chicken hepatocytes by inhibiting CYP450 1A5 expression via upregulated SelW expression. Journal of Agricultural and Food Chemistry 65: 2495–2502.

8. Cheng L, He W, Gong H, Wang C, Chen Q, Cheng Z, Liu Z (2013) PEGylated micelle nanoparticles encapsulating a non-fluorescent near-infrared organic dye as a safe and highly-effective photothermal agent for in vivo cancer therapy. Advanced Functional Materials 23: 5893–5902.
9. Chrysels PL, Andres CJ, Allen PG (2011) DNA ligands for aflatoxin and zearalenone. p. WO 2011/020198A1.
10. Fu G, Sanjay S, Zhou W, Brekken R, Kirken R, Li X (2018) Exploration of nanoparticle-mediated photothermal effect of TMB-H_2O_2 colorimetric system and its application in a visual quantitative photothermal immunoassay. Analytical Chemistry 90: 5930–5937.
11. Fu Y, Xiao K, Zhang X, Du C, Chen J (2021) Peptide cleavage-mediated and environmentally friendly photocurrent polarity switching system for prostate-specific antigen assay. Analytical Chemistry 93: 1076–1083.
12. Goud K, Sharma A, Hayat A, Catanante G, Gobi K, Gurban A, Marty J (2016) Tetramethyl-6-carboxyrhodamine quenching-based aptasensing platform for aflatoxin B1: analytical performance comparison of two aptamers. Analytical Biochemistry 508: 19–24.
13. Hansen J, Wang J, Kawde A, Xiang Y, Gothelf K, Collins G (2006) Quantum-dot/aptamer-based ultrasensitive multi-analyte electrochemical biosensor. Journal of the American Chemical Society 128: 2228–2229.
14. Hao N, Lu J, Zhou Z, Hua R, Wang K (2018) A pH-resolved colorimetric biosensor for simultaneous multiple target detection. ACS Sensors 3: 2159–2165.
15. Liu H, Bai Y, Qin J, Wang H, Wang Y, Chen Z, Feng F (2018) Exonuclease I assisted fluorometric aptasensor for adenosine detection using 2-AP modified DNA. Sensors and Actuators B: Chemical 256: 413–419.
16. Luo L, Ma S, Li L, Liu X, Zhang J, Li X, Liu D, You T (2019) Monitoring zearalenone in corn flour utilizing novel self-enhanced electrochemiluminescence aptasensor based on NGQDs-NH_2-Ru@SiO_2 luminophore. Food Chemistry 292: 98–105.
17. Luo M, Xue X, Rao H, Wang H, Liu X, Zhou X, Xue Z, Lu X (2020) Simply converting color signal readout into thermal signal readout for breaking the color resolution limitation of colorimetric sensor. Sensors and Actuators B: Chemical 309: 127707.
18. Pradhan N, Battaglia D, Liu Y, Peng X (2007) Efficient, stable, small, and water-soluble doped ZnSe nanocrystal emitters as non-cadmium biomedical labels. Nano Letters 7: 312–317.
19. Seok Y, Byun J, Shim W, Kim M (2015) A structure-switchable aptasensor for aflatoxin B1 detection based on assembly of an aptamer/split DNAzyme. Analytica Chimica Acta 886: 182–187.
20. Wang B, Chen Y, Wu Y, Weng B, Liu Y, Lu Z, Li C, Yu C (2016) Aptamer induced assembly of fluorescent nitrogen-doped carbon dots on gold nanoparticles for sensitive detection of AFB1. Biosensors and Bioelectronics 78: 23–30.
21. Wang C, Huang X, Tian X, Zhang X, Yu S, Chang X, Ren Y, Qian J (2019) A multiplexed FRET aptasensor for the simultaneous detection of mycotoxins with magnetically controlled graphene

oxide/Fe_3O_4 as a single energy acceptor. Analyst 144: 6004–6010.

22. Wang C, Qian J, An K, Ren C, Lu X, Hao N, Liu Q, Li H, Huang X, Wang K (2018) Fabrication of magnetically assembled aptasensing device for label-free determination of aflatoxin B1 based on EIS. Biosensors and Bioelectronics 108: 69–75.
23. Wang C, Qian J, Wang K, Yang X, Liu Q, Hao N, Wang C, Dong X, Huang X (2016) Colorimetric aptasensingofochratoxinAusingAu@Fe_3O_4 nanoparticles as signal indicator and magnetic separator. Biosensors and Bioelectronics 77: 1183–1191.
24. Wang C, Qian J, Wang K, Hua M, Liu Q, Hao N, You, T, Huang X (2015) Nitrogen-doped graphene quantum dots@SiO_2 nanoparticles as electrochemiluminescence and fluorescence signal indicators for magnetically controlled aptasensor with dual detection channels. ACS Applied Materials & Interfaces 7: 26865–26873.
25. Wang C, Qian J, Wang K, Wang K, Liu Q, Dong X, Wang C, Huang X (2015) Magnetic-fluorescent-targeting multifunctional aptasensor for highly sensitive and one-step rapid detection of ochratoxin A. Biosensors and Bioelectronics 68: 783–790.
26. Woo M, Kim M, Jung J, Park K, Seo T, Park H (2013) A novel colorimetric immunoassay utilizing the peroxidase mimicking activity of magnetic nanoparticles. International Journal of Molecular Sciences 14: 9999–10014.
27. Xia X, Wang H, Yang H, Deng S, Deng R, Dong Y, He Q (2018) Dual-terminal stemmed aptamer beacon for label-free detection of aflatoxin B1 in broad bean paste and peanut oil via aggregation-induced emission. Journal of Agricultural and Food Chemistry 66: 12431–12438.
28. Xie H, Zhen R, Wang B, Feng Y, Chen P, Hao J (2010) Fe_3O_4/Au core/shell nanoparticles modified with Ni^{2+}–nitrilotriacetic acid specific to histidine-tagged proteins. Journal of Physical Chemistry C 114: 4825–4830.
29. Xie S, Chai Y, Yuan Y, Bai L, Yuan R (2014) Development of an electrochemical method for ochratoxin A detection based on aptamer and loop-mediated isothermal amplification. Biosensors and Bioelectronics 55: 324–329.
30. Xing K, Shan S, Liu D, Lai W (2020 Recent advances of lateral flow immunoassay for mycotoxins detection. Trends in Analytical Chemistry 133: 116087.
31. Xiong Y, Pei K, Wu Y, Duan H, Lai W, Xiong Y (2018) Plasmonic ELISA based on enzyme-assisted etching of Au nanorods for the highly sensitive detection of aflatoxin B1 in corn samples. Sensors and Actuators B: Chemical 267: 320–327.
32. Xiong X, Yuan W, Li Y, Lu Y, Xiong X, Li Y, Liu Y, Lu L (2020) Sensitive electrochemical detection of aflatoxin B1 using DNA tetrahedronnanostructure as substrate of antibody ordered assembly and template of aniline polymerization. Food Chemistry 331: 127368.
33. Xue Z, Zhang Y, Yu W, Zhang J, Wang J, Wan F, Kim Y, Liu Y, Kou X (2019) Recent advances in aflatoxin B1 detection based on nanotechnology and nanomaterials-A review. Analytica Chimica Acta 1069: 1–27.

34. Yang C, Wang Y, Marty J, Yang X (2011) Aptamer-based colorimetric biosensing of Ochratoxin A using unmodified gold nanoparticles indicator. Biosensors and Bioelectronics 26: 2724–2727.
35. Yang X, Shi D, Zhu S, Wang B, Zhang X, Wang G (2018) Portable Aptasensor of aflatoxin B1 in bread based on a personal glucose meter and DNA walking machine. ACS Sensors 3: 1368–1375.
36. Zhang J, Chen J, Zhang X, Zeng Z, Wang S (2012) An electrochemical biosensor based on hairpin-DNA aptamer probe and restriction endonuclease for ochratoxin A detection. Electrochemistry Communications 25: 5–7.
37. Zheng M, Yue C, Ma Y, Gong P, Zhao P, Zheng C, Sheng Z, Zhang P, Wang Z, Cai L (2013) Single-step assembly of DOX/ICG loaded lipid-polymer nanoparticles for highly effective chemo-photothermal combination therapy. ACS Nano 7: 2056–2067.
38. Zheng W, Teng J, Cheng L, Ye Y, Pan D, Wu J, Xue F, Liu G, Chen W (2016) Hetero-enzyme-based two-round signal amplification strategy for trace detection of aflatoxin B1 using an electrochemical aptasensor. Biosensors and Bioelectronics 80: 574–581.

Scheme

Scheme 1 is available in the Supplementary Files section

Figures

Figure 1

TEM images of the Au@Fe_3O_4 (A) and (B). (C) XRD patterns of the as-prepared Au@Fe_3O_4 MB (a), Fe_3O_4 (b), and Au (c). (D) Magnetic hysteresis loops of pure Fe_3O_4 (a) and Au@Fe_3O_4 (b) NPs. Inset: the separation and re-dispersion process of Au@Fe_3O_4.

Figure 2

(A) UV–vis spectra of free cDNA (a), Au@Fe_3O_4 (b), and cDNA-MB (c). (B) CV curves of ITO (a) and ITO/AuNPs in 0.5 M H_2SO_4. (C) P 2p XPS spectra of ITO/AuNPs before (a) and after (b) aptamer conjugation. (D) Concentration influence of aptamer for the performance of the ITO/AuNPs.

Figure 3

Influence of time (A) and concentration (C) for the performance between cDNA-MB and Apt-ITO/AuNPs. (B) EIS of ITO/AuNPs (a), Apt-ITO/AuNPs (b), Apt-ITO/AuNPs-MCH (c), and MB-Apt/cDNA-ITO/AuNPs (d) modified glass in 5.0 mM $Fe(CN)_6^{3-/4-}$ containing 0.1 M KCl at 100 mV s^{-1}. Inset of B: the equivalent circuit. (D) Influence of the incubation time and temperature for the performance of the aptasensor upon the incubation of 50 pg mL^{-1} AFB1.

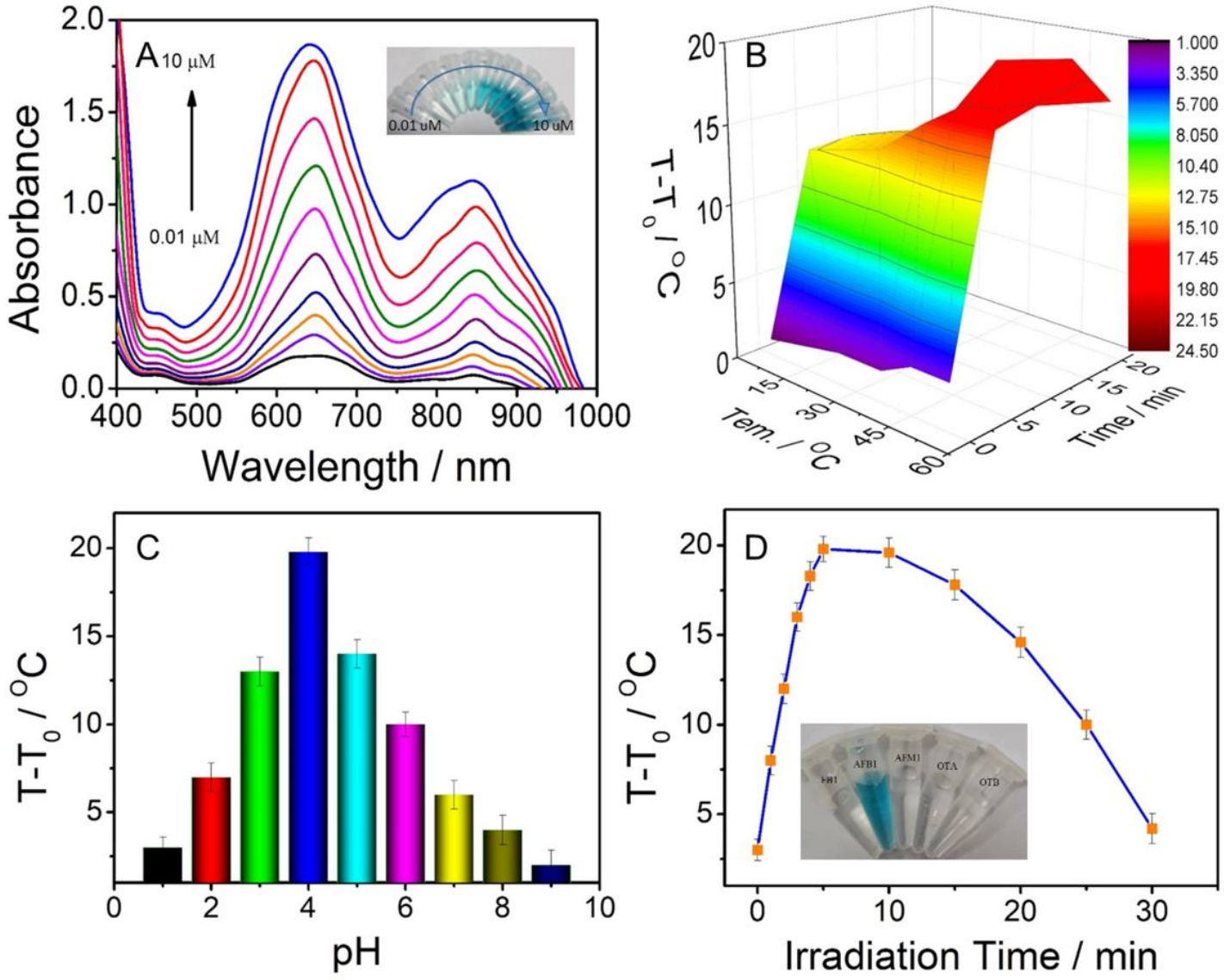

Figure 4

Vis-NIR spectra of 250 μM TMB reaction solutions upon different $Au@Fe_3O_4$ concentrations (A). Influence of the reaction time and temperature for the Vis-NIR of the TMB upon the 50 μM $Au@Fe_3O_4$ (B). Influence of pH for the Vis-NIR of the TMB upon the 50 μM $Au@Fe_3O_4$ (C). The effect of irradiation time on aptasensor performance (D). Inset: The responses of the aptasensor with different targets.

Figure 5

(A) EIS profiles of the aptasensor corresponding to various AFB1 concentrations (from a to h: 0, 0.1, 1, 20, 100, 200, 300, and 500 ng mL^{-1}). (B) Relationship between △Ret and the different concentrations of AFB1. Inset: the calibration curve for the EIS assay. (C) Temperature of the proposed aptasensor systems upon various AFB1 concentrations (from a to i: 0, 0.01, 0.1, 1, 10, 50, 100, 200, and 300 ng mL^{-1}). (D) Relationship between T-To and the different concentrations of AFB1. Inset: Calibration curve for AFB1 determination.

Supplementary Files

This is a list of supplementary files associated with this preprint. Click to download.

- Scheme1.png